Chemical Science

ROYAL SOCIETY OF CHEMISTRY

EDGE ARTICLE

View Article Online
View Journal

Cite this: DOI: 10.1039/d6sc03059a

All publication charges for this article have been paid for by the Royal Society of Chemistry

One- and two-electron coordinatively-induced reduction of *N*-heterocycles by divalent rare earth terphenyl anilide complexes

Ross E. MacKenzie,[ab] Benjamin L. L. Réant,[ab] Iain J. Cameron,[ab] Harry M. Silver,[ab] George F. S. Whitehead,[b] Eric J. L. McInnes[b] and Conrad A. P. Goodwin *[ab]

Received 13th April 2026
Accepted 8th June 2026

DOI: 10.1039/d6sc03059a

rsc.li/chemical-science

Molecular rare-earth (RE) complexes in the divalent oxidation state have been used as potent one-electron reductants, yielding bonding motifs not accessible elsewhere in the periodic table. A deeper understanding of the chemical properties which dictate their reducing power is required to tame their reduction potentials and unlock new controlled reactivity. Here, we report the electrochemical characterisation of a series of divalent *bis*-(tethered)arene complexes, [M^{II}(NHAr^{iPr6})$_2$] (**1M**, M = Y, La, Sm, Eu, Yb, Tm, Lu; NHAr^{iPr6} = {N(H)C$_6$H$_3$-2,6-(C$_6$H$_2$-2,4,6-*i*Pr$_3$)$_2$}), and their reactivity towards the nitrogen heterocycles pyridine and 4,4′-bipyridine. Complexes **1Y**, **1La**, **1Tm**, and **1Lu** reduce 4,4′-bipyridine and reductively couple pyridine to afford the dimeric [{M^{III}(NHAr^{iPr6})$_2$}$_2$(μ-N$_2$C$_{10}$H$_8$)] (**2M**, M = Y, La, Tm, Lu) and [{M^{III}(NHAr^{iPr6})$_2$}$_2$(μ-N$_2$C$_{10}$H$_{10}$)] (**3M**, M = Y, La, Tm, Lu) respectively. These results contrast with electrochemical measurements, which place the RE(III/II) reduction potentials for all **1M** complexes as insufficiently reducing for either heterocycle. These results imply the reactions proceed through coordination-induced reduction. Synthesis of **2M** complexes also results in the formation of 4,4′-bipyridine radical species, which are probed by NMR, EPR, and UV-vis-NIR spectroscopies.

Introduction

Fundamental understanding of the redox chemistry of rare-earth (RE) elements has lagged behind that of the transition metals and early actinides. Initial research was limited to Sm(II) (f^6), Eu(II) (f^7), and Yb(II) (f^{14}) given the increased stability gained from the filled, half-filled, or near half-filled subshells, respectively.[1] The isolation of a molecular Tm(II) species in 1997,[2] followed by Dy(II),[3] and Nd(II),[4] showed that it was not only the three "classical" divalent rare earths, samarium, europium, and ytterbium, that could yield isolable molecular divalent compounds. Subsequent work has extended the range of known RE(II) molecules to include the entire series, except for radioactive promethium,[5] and two distinct electronic structures have emerged: those with f^{n+1} electron configurations, or those with f^n d^1 configurations (4d^1 and 3d^1 for Y and Sc respectively, 5d^1 for lanthanides, Fig. 1). By-and-large, the former encompasses all Sm(II), Eu(II), and Yb(II) complexes, Tm(II),[6] Dy(II), and Nd(II)[7–10] exist at an interface where ligands and coordination geometry direct the ground-state configuration, and all other RE(II) ions exhibit f^n d^1 configurations.[11–25] Moreover, of those complexes with formal f^n d^1 configurations, some have been reported where the highest singly-occupied molecular orbital (SOMO) resembles a {(*n* + 1)s(*n*d$_z^2$)} hybrid atomic orbital (*e.g.* {6s(5d$_z^2$)}),[11–20,26] and others where the SOMO has significant ligand-character, most commonly with arene rings,[21–25] which can be used to trap masked low-oxidation state synthons.[27–38]

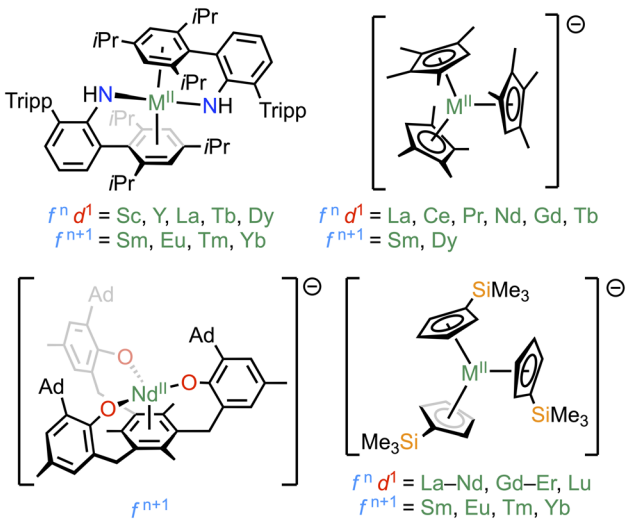

Fig. 1 Select examples of RE(II) complexes showing examples of f^{n+1} and f^n d^1 valence electron configurations, and how these change depending on the coordination environment.

[a]*Centre for Radiochemistry Research, The University of Manchester, Oxford Road, Manchester, M13 9PL, UK. E-mail: conrad.goodwin@manchester.ac.uk*

[b]*Department of Chemistry, The University of Manchester, Oxford Road, Manchester, M13 9PL, UK*

Owing to their large, negative reduction potentials, divalent rare-earth ions have been used as strong reducing agents capable of performing single-electron transfer (SET) reactions, such as the reduction of N_2,[39,40] CO,[41,42] alkynes,[43,44] and nitrogenous heterocycles.[45–49] While the number of divalent rare-earth complexes has grown considerably, electrochemical studies have been limited by the low reduction potentials and high reactivity of these ions. The $[RE^{III}(Cp')_3]$ ($Cp' = \{C_5H_4SiMe_3\}$) motif is known for all RE elements save scandium and promethium,[8,11,14–16,50] which makes it ideal to explore trends in the RE(III/II) reduction potential ($E_{1/2}$) across these elements.[51] Across the lanthanide members in this series, the reduction potentials (*vs.* $[Fe(Cp)_2]^{+/0}$, $Cp = \{C_5H_5\}$) for the $4f^{n+1}$ ions follow the expected trend based on the stability of their electronic configurations:[1] Eu(II) $4f^7$ (−1.07 V) > Yb(II) $4f^{14}$ (−1.64 V) > Sm(II) $4f^6$ (−2.41 V) > Tm(II) $4f^{13}$ (−2.83 V), while the non-traditional $4f^n$ $5d^1$ ions exhibit more negative reduction potentials that fall within a narrow range (−2.95 V to −3.14 V). This is due to their electronic structures, where the highest-occupied molecular orbital is largely non-bonding, resembling a $\{6s(5d_z^2)\}$ hybrid atomic orbital oriented perpendicular to the molecular C_3-axis. As such, the ligands, which remain constant across the series, define the splitting of the d-orbital manifold, and hence the energy and reducing power of the configuration, so the RE identity has little influence on the reduction potential for these non-traditional RE(II) ions.

We recently reported $[M^{II}(NHAr^{iPr6})_2]$ (M = Sc, Y, La, Sm, Eu, Tm, Yb; $NHAr^{iPr6} = \{NHC_6H_3\text{-}2,6\text{-}Tripp_2\}$, $Tripp = \{C_6H_2\text{-}2,4,6\text{-}iPr_3\}$) as a series of neutral, room-temperature-stable, divalent rare-earth complexes covering both the $4f^{n+1}$ (Sm, Eu, Tm, and Yb) and f^n d^1 (Sc, Y, and La where $n = 0$) configurations.[25] In the case of Sc(II), Y(II), and La(II), significant metal–ligand orbital mixing between flanking arene groups and the metal centre gives rise to a one-electron δ-bonding interaction.[25] The balance of metal and ligand character in this interaction varies with the metal identity, unlike in RE(II) complexes with a non-bonding $\{ns(n-1d)\}$ configuration, which means the reducing power of these complexes might be modulated by the metal identity – but this concept remains unexplored at present.

Herein, we present an electrochemical study of the $[M^{II}(NHAr^{iPr6})_2]$ (**1M**, M = Y, La, Sm, Eu, Tm, Yb, Lu) complexes, and their reactivity towards two *N*-heterocycles – 4,4′-bipyridine and pyridine – which have well-defined one- and two-electron redox chemistry in order to quantify their chemical reducing power alongside electrochemical measurements. Well-defined quasi-reversible RE(III/II) couples are found with six of the seven complexes, with **1Eu** showing no redox events by cyclic voltammetry. The most reducing examples, (**1Y**, **1La**, **1Lu**, and **1Tm**) reduce 4,4′-bipyridine to its dianion in bimetallic $[\{M^{III}(NHAr^{iPr6})_2\}_2(\mu\text{-}N_2C_{10}H_8)]$ (**2M**, M = Y, La, Tm, Lu), and also reduce pyridine to a radical which subsequently undergoes $C_{(sp^3)}$–$C_{(sp^3)}$ coupling to give bimetallic $[\{M^{III}(NHAr^{iPr6})_2\}_2(\mu\text{-}N_2C_{10}H_{10})]$ (**3M**, M = Y, La, Tm, Lu). The less reducing examples (**1Sm**, **1Eu**, and **1Yb**) do not reduce either heterocycle, and spectroscopic investigations (UV-vis-NIR, NMR) suggest that the metal centres do not coordinate to the heterocycles in solution with these metals.

Results

Synthesis and electrochemistry

The divalent complexes **1M** (M = Y, La, Sm, Eu, Tm, Yb, Lu) were prepared by the KC_8-mediated reduction of trivalent iodide precursors, $[M^{III}(NHAr^{iPr6})_2(I)]$, or directly from divalent metal iodides, using methods described previously.[25] Cyclic voltammetry was performed on all **1M** complexes (M = Y, La, Sm, Eu, Tm, Yb, Lu) under an argon atmosphere as 10 mM solutions in THF with $[nBu_4N][BPh_4]$ (50 mM) as the electrolyte with a glassy carbon working electrode, platinum wire counter electrode, and a Ag/AgCl pseudo-reference electrode. All data is reported with reference to the $[Fc]^{+/0}$ couple (Fc = $[Fe(Cp)_2]$; Cp = $\{C_5H_5\}$). Solutions of **1M** are unstable in the presence of Fc, though we have not been able to characterise the products of the reaction. Therefore, the $[Fc^*]^{+/0}$ ($Fc^* = [Fe(Cp^*)_2]$; $Cp^* = \{C_5Me_5\}$) couple was used instead to provide an internal reference standard for all measurements, which was then calibrated to the $[Fc]^{+/0}$ couple.[52–55] The use of an internal standard is essential to the reliable determination of the reduction potential of these species. The SI (Section 7) contains full scans used for referencing each complex.

Cyclic voltammograms for **1Sm**, **1Tm**, and **1Yb** give $E_{1/2}$ values for the $[M(NHAr^{iPr6})_2]^{+/0}$ couple that correlate well with the standard reduction potentials for each ion,[56] in order from least to most cathodic: **1Yb** (−1.20 V) > **1Sm** (−1.51 V) > **1Tm** (−2.04 V). The $E_{1/2}$ values for the complexes with formal $4f^n$ $5d^1$ configurations fall within a small range: **1Y** (−2.32 V; $4d^1$), **1La** (−2.24 V), and **1Lu** (−2.20 V), but are all somewhat more cathodic than those with $4f^{n+1}$ configurations. The trend is analogous to that of the $[RE^{III}(Cp')_3]$ series;[51] however, in every case, $E_{1/2}$ for the RE(III/II) couple in the **1M** series is more anodic. A summary of the RE(III/II) potentials is given in Table 1, and in Fig. 2 shows scans for each **1M** complex (save **1Eu**). In the case of **1Eu**, no redox events were observed that could be definitively assigned to **1Eu**, despite repeated attempts under both light and dark conditions. An irreversible oxidation wave could be seen at a moderately anodic potential (+0.14 V *vs.* $[Fc]^{+/0}$), which overlapped with the oxidation wave of our electrochemical standard (Fc*; see Fig. S119).

For each **1M** complex (save **1Eu**), a second quasi-reversible reduction event was observed at more negative potentials (from −2.60 V to −3.76 V, see Fig. S50), the order of which is roughly the inverse of the trend in their M(III/II) potentials – *i.e.*

Table 1 Summary of electrochemical data for **1M** (M = Y, La, Lu, Tm, Sm, Yb). Potentials given *vs.* $[Fc]^{+/0}$, and all data derived from scans at 200 mV s^{-1}

Complex	$E_{1/2}$ $[M^{II}(NHAr^{iPr6})_2]^{+/0}$ (V)	E_{pa} (V)	E_{pc} (V)	ΔE_p (mV)
1Y	−2.32	−2.19	−2.45	260
1La	−2.24	−1.95	−2.53	580
1Lu	−2.20	−2.08	−2.32	240
1Tm	−2.04	−1.84	−2.24	400
1Sm	−1.51	−1.34	−1.68	340
1Yb	−1.20	−0.87	−1.53	660

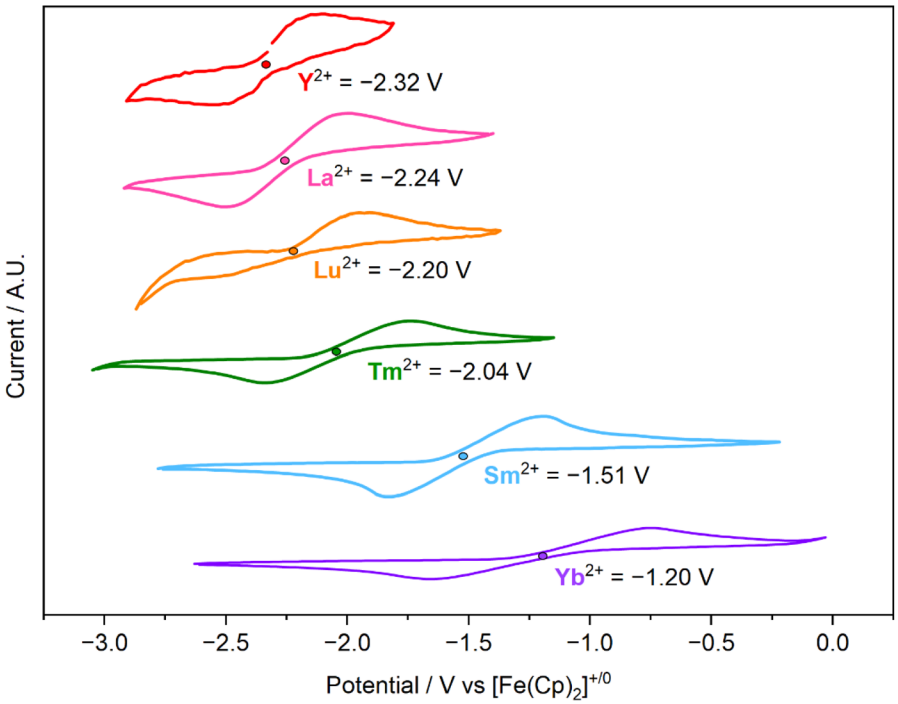

Fig. 2 Cyclic voltammograms of **1M** (M = Y, La, Lu, Tm, Sm, Yb) in THF (10 mM) supported by [nBu$_4$N][BPh$_4$] (50 mM) *vs.* [Fc]$^{+/0}$ at 200 mV s^{-1}.

the second event in **1Yb** is the most cathodic, and with **1Y**, **1La**, and **1Lu**, it is the most anodic.

Spectroscopic assessment of reducing power in solution

The nitrogen heterocycles 4,4′-bipyridine and pyridine have one- and two-electron (−2.32 V, −2.88 V), and one-electron (−3.22 V), reduction potentials,[57–60] respectively (Scheme 1), that are close to, or more negative than, the M(III/II) couples in the **1M** complexes herein (range: −1.20 V to −2.32 V). We first used NMR spectroscopy and UV-vis-NIR titration studies to assess reactions between solutions of **1M** (M = Y, La, Sm, Eu, Tm, Yb, Lu) and both pyridine and 4,4′-bipyridine.

^{1}H NMR spectra of diamagnetic **1Yb** and 4,4′-bipyridine or pyridine in d_6-benzene showed no change compared to that of **1Yb** (Fig. S133–135) The paramagnetic nature of **1Sm** and **1Eu** renders their ^{1}H NMR spectra largely uninformative; however, d_6-benzene solutions of either **1Sm** or **1Eu** in the presence of 4,4′-bipyridine or pyridine showed no change to their NMR spectra (see Table S10), which suggests their oxidation states remain unchanged. UV-vis-NIR spectra were collected for all three complexes (Fig. S136–S138) in toluene in the presence of 4,4′-bipyridine or pyridine. These spectra showed no significant differences compared to those of isolated **1Sm**, **1Eu**, or **1Yb**. Together, these data indicate that 4,4′-bipyridine and pyridine are not reduced by these complexes and are unlikely to coordinate to the metal centre.

Titration of 4,4′-bipyridine into d_6-benzene solutions of **1Y**, **1La**, or **1Lu**, gave diamagnetic ^{1}H NMR signals consistent with the 4,4′-bipyridine dianion at *ca.* 5.8 ppm and 5.6 ppm ($^3J_{HH}$ = 7 Hz for both).[49,61] With **1Y** and **1Lu**, the intensity of these resonances decreased rapidly as the concentration of 4,4′-bipyridine was increased. Once more than 0.5 equivalents were added, new signals appeared at δ_H = 8.56 and 6.81 ppm, corresponding to neutral 4,4′-bipyridine. In the case of **1La**, signals from the 4,4′-bipyridine dianion do not disappear with increased quantities of 4,4′-bipyridine dianion, but neutral 4,4′-bipyridine was observed (see Fig. S139–S141).

UV-vis-NIR titration experiments were performed on **1M** (M = Y, La, Tm, Lu) in toluene, ranging from 0 to >0.8 equivalents of 4,4′-bipyridine (Fig. 3). Starting with **1La**, at low

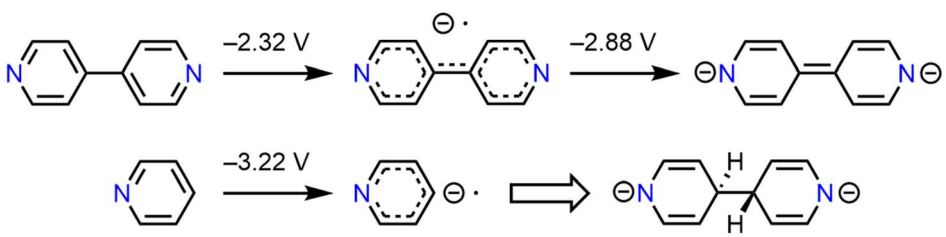

Scheme 1 Reduction potentials for 4,4′-bipyridine and pyridine *versus* the [Fc]$^{+/0}$ couple, and see Fig. S122–S125 for measurements.[57–60]

concentrations of 4,4′-bipyridine, the UV-vis-NIR spectrum shows the appearance of strong broad absorbances at 408 nm (24 500 cm^{-1}, $\varepsilon = 7.28 \times 10^3$ M^{-1} cm^{-1}) and 600 nm (16 700 cm^{-1}, $\varepsilon = 1.76 \times 10^3$ M^{-1} cm^{-1}), which increase in intensity as the concentration of 4,4′-bipyridine increases up to *ca.* 0.5 equivalents, before decreasing beyond this. With **1Y** and **1Tm** (Fig. S149–S152), UV-vis-NIR spectra after the addition of 0.1 equivalents of 4,4′-bipyridine are similar to those of **1La** – showing broad absorbances at 382 nm (24 500 cm^{-1}: **1Y** $\varepsilon = 8.9 \times 10^3$ M^{-1} cm^{-1}, **1Tm** $\varepsilon = 12.6 \times 10^3$ M^{-1} cm^{-1}) and 610 nm (16 393 cm^{-1}: **1Y** $\varepsilon = 3.0 \times 10^3$ M^{-1} cm^{-1}, **1Tm** $\varepsilon = 5.1 \times 10^3$ M^{-1} cm^{-1}). However, higher concentrations (>0.3 equivalents) of 4,4′-bipyridine cause the features to blue-shift slightly, and the appearance of fine structure in the low-energy region in the spectra for both complexes, which is resolved into two broad peaks (586 nm, 17 065 cm^{-1} and 632 nm, 15 823 cm^{-1}). In the case of **1Lu**, the fine structure was apparent in all spectra, even at the lowest concentrations of 4,4′-bipyridine. Solutions of **1Y**, **1La**, **1Tm**, and **1Lu** are green in the presence of low concentrations of 4,4′-bipyridine, but at higher concentrations, those with **1Y**, **1Tm**, and **1Lu** turn blue. These spectra are all similar to that of the 4,4′-bipyridinyl radical anion and the 4,4′-bipyridine dianion,[62–66] and to an organoboron compound featuring a 4,4′-bipyridine core in three oxidation states,[61] but are different to several other metal complexes featuring 4,4′-bipyridine anions.[49,67]

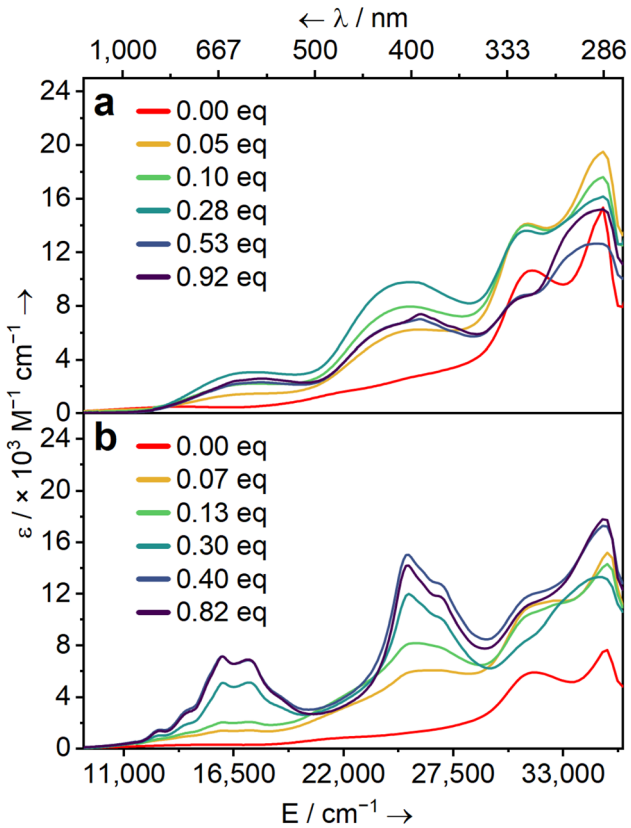

Fig. 3 UV-vis-NIR spectra for titration experiments on **1La** (a) and **1Lu** (b). Each line denotes the number of equivalents of 4,4′-bipyridine added to the solution of **1La** or **1Lu**.

The addition of pyridine to solutions of the **1M** complexes (M = Y, La, Tm, Lu) resulted in rapid, irreversible colour changes from dark red/green to yellow in all cases.

It is evident from ^{1}H NMR and UV-vis-NIR titration data that **1Y**, **1La**, **1Tm**, and **1Lu** react with 4,4′-bipyridine to form a product containing the 4,4′-bipyridine dianion, but, except for **1La**, each reacts further to give another species that forms even at low concentrations of 4,4′-bipyridine. While the reduction potentials of 4,4′-bipyridine and pyridine are more negative than the [naphthalene]$^{0/-}$ couple (−2.2 V *vs.* $[Fc]^{+/0}$),[68] and other RE(II) complexes reduce a range of neutral aromatic hydrocarbons,[3,69–77] no reaction was observed between **1M** (M = Y, La, Lu) and naphthalene or anthracene (−1.9 V *vs.* $[Fc]^{+/0}$)[68] by NMR spectroscopy (see Fig. S142–S147).

Preparative-scale reactions with 4,4′-bipyridine and pyridine

The reaction between two equivalents of **1M** (M = Y, La, Tm, Lu) and one equivalent of 4,4′-bipyridine in toluene resulted in a rapid colour change from dark red/green to intense royal blue (M = Y, Tm, Lu) or dark green (M = La). Work-up and crystallisation from *n*-hexane gave the bimetallic [{M^{III}(NHAr^{iPr6})$_2$}$_2$(μ-$N_2C_{10}H_8$)] (**2M**, M = Y, La, Tm, Lu) complexes in poor to fair isolated crystalline yields (25–48%) (Scheme 2). Similarly, the addition of pyridine to a toluene solution containing an equimolar amount of **1M** (M = Y, La, Tm, Lu) produced an immediate colour change from dark red to yellow. Workup and crystallisation from *n*-hexane gave bimetallic [{M^{III}(NHAr^{iPr6})$_2$}$_2$(μ-$N_2C_{10}H_{10}$)] (**3M**, M = Y, La, Tm, Lu) complexes in poor to fair crystalline yields (22–52%) (Scheme 2). Similar reactions with **1Sm**, **1Eu**, and **1Yb** gave the starting materials unchanged.

^{1}H NMR spectra of isolated **2M** (M = Y, La, Lu) in d_6-benzene show they are diamagnetic, exhibiting two resonances at δ_H = 5.8 (*d*, 4H, $^3J_{HH}$ = 7.3 Hz) and 5.6 (*d*, 4H, $^3J_{HH}$ = 7.5 Hz) corresponding to the 2,2′,6,6′ and 3,3′,5,5′ protons of the 4,4′-bipyridyl dianion unit respectively, and are therefore twofold symmetric in solution (Fig. S10–S19). The resonances are shifted upfield relative to those of neutral 4,4′-bipyridine, suggesting reduction and a loss of aromaticity (Scheme 1). For **2Tm**, the solution-state molar magnetic susceptibility was found to be 6.07 μ_B (using the Evans method), somewhat lower than the typical range for Tm(III) (7.1–7.5 μ_B), but consistent with previous observations of dimeric Tm(III) complexes [{Tm^{III}($C_4H_{10}O_2$)(η^2-$C_{10}H_8$)}$_2$(η^4-$C_{10}H_8$)] (6.59 μ_B) and [{Tm^{III}(I)$_2$(C_5H_5N)$_4$}$_2$(μ-$N_2C_{10}H_{10}$)] (6.05 μ_B).[78,79] The ^{1}H NMR spectra for **3Y**, **3La**, and **3Lu** are consistent with diamagnetic compounds, with three resonances at δ_H = 6.0 (s, 4H), 4.6 (m, 4H), 3.4 (s, 2H), consistent with single electron transfer from the metal centre to the pyridine substituent, followed by C–C coupling at the para position (Fig. S20–S28).

The solution molar magnetic susceptibility for **3Tm** (7.5 μ_B) is in excellent agreement with the theoretical value for two non-interacting Tm(III) ions. Solution UV-vis-NIR spectra for isolated **2M** (M = Y, La, Tm, Lu) show similar features to the titration studies, whereby **2La** shows two broad features without fine structure, which is consistent with the 4,4′-bipyridyl dianion,

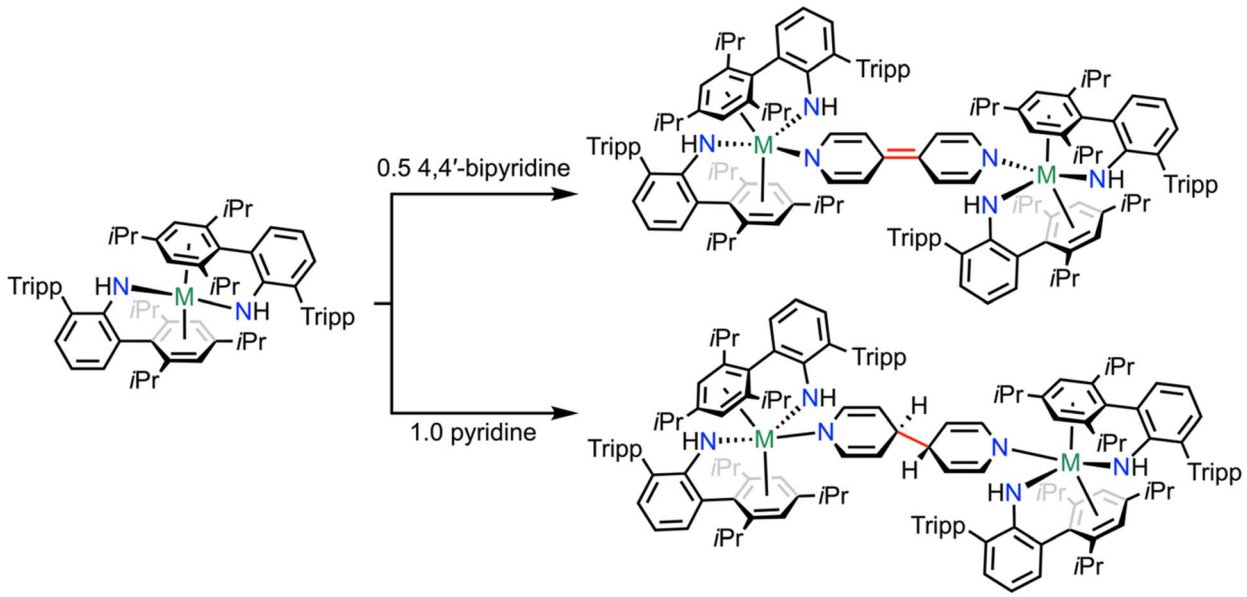

Scheme 2 The synthesis of **2M** (M = Y, La, Tm, Lu) and **3M** (M = Y, La, Tm, Lu) complexes, from the reduction of 4,4′-bipyridine or pyridine with **1M** (M = Y, La, Tm, Lu) complexes.

whereas the spectra of **2Y**, **2Tm**, and **2Lu** all show additional features that resemble the 4,4′-bipyridyl radical anion (Fig. S37–S40).[61–64] Solid-state UV-vis-NIR spectra of all four complexes showed no significant differences (Fig. S41–S44). Solution UV-vis-NIR spectra of all **3M** (M = Y, La, Tm, Lu) complexes are largely featureless, with an intense band extending from the UV region to *ca.* 20 000 cm^{-1}, which accounts for their strong yellow colouration. The spectrum of **3Tm** also features two sharp but weak absorbances at 12 797 cm^{-1} (781 nm, $\varepsilon = 15\ M^{-1}\ cm^{-1}$) and 14 701 cm^{-1} (680 nm, $\varepsilon = 7\ M^{-1}\ cm^{-1}$) corresponding to the $^3H_6 \rightarrow {}^3F_4$ and $^3H_6 \rightarrow {}^3F_{2/3}$ transitions typical for a Tm(III) ion.[80]

Molecular structures

Single-crystal X-ray diffraction studies of all **2M** and **3M** complexes reveal that they are pseudo-3-coordinate, considering only the anionic donors. The structures of **2La** and **3La** are shown in Fig. 4 as examples; see the SI (Section 2) for all others.

Complexes **2Y** and **2Lu** crystalise in the monoclinic space group $P2_1/c$ ($Z' = 0.5$) with an inversion through the central C–C bond of the bipyridyl unit. Complex **2Tm** crystalised in the orthorhombic space group $Cmc2_1$ ($Z' = 0.5$), and **2La** crystalised in the orthorhombic *Cmce* space group with one quarter of the dimeric molecule per asymmetric unit ($Z' = 0.25$). The most notable feature of **2M** complexes is the short central C–C bond length (**2Y**, 1.355(18) Å; **2La**, 1.389(8) Å; **2Tm**, 1.323(11) Å; **2Lu**, 1.368(4) Å) that are consistent with a C–C double bond and suggest the reduction of 4,4′-bipyridine to its dianion (Scheme 1), consistent with the upfield shift for the bipyridyl protons in the ^{1}H NMR spectra.[49,61,81,82] The M–N_{bipy} bond lengths (**2Y**, 2.211(7) Å; **2La**, 2.336(3) Å; **2Tm**, 2.174(5) Å; **2Lu**, 2.1613(16) Å) are considerably shorter than those of neutral 4,4′-bipyridine adducts to these metals,[83–88] and are typical for M–N distances to anionic N-donors. In the solid state, the La-centre in **2La** retains coordination to two Tripp substituents, whereas for **2Y**, **2Tm**, and **2Lu** only one remains bound to accommodate the 4,4′-bipyridine unit. However, the ^{1}H NMR spectra for all show that this interaction is fluxional on the NMR timescale.

Complexes **3Y** and **3Lu** crystallised in the monoclinic space groups $P2_1/n$ and $P2_1$ ($Z' = 1$) respectively, whereas **3La** and **3Tm** crystallised in the triclinic space group $P\bar{1}$ ($Z' = 1$). The structural data confirm **3M** complexes possess a new coupled C–C single bond (lengths: **3Y**, 1.564(5) Å; **3La**, 1.558(11) Å; **3Tm**, 1.560(4) Å; **3Lu**, 1.541(7) Å) at the para position of the pyridine moieties. The two M–N_{py} bond distances are statistically indistinguishable from one another, but are shorter than neutral pyridine adducts with these metals, suggesting they are anionic N-donors.[89–91] As with the **2M** complexes, **3Y**, **3Tm**, and **3Lu** each have one bound Tripp ring, while **3La** maintains close contact with two Tripp rings. In **3Y**, **3Tm**, and **3Lu**, the twist about the central C–C single bond is small (N···C–C···N torsion angle = **3Y**, 59.0(3)°; **3Tm**, 63.1(4)°; **3Lu**, 60.9(6)°), whereas in **3La** the two pyridyl units adopt a stepped configuration (N···C–C···N torsion angle = 173.9(14)°).

Radical formation in 2M complexes

Although **2M** (M = Y, La, Lu) are diamagnetic (see above), frozen-solution and powder electron paramagnetic resonance (EPR) spectroscopy measurements gave signals consistent with the presence of radical species (see Fig. S153–S162). The signals observed in the solution spectra of **2La** and **2Tm** were very weak and significantly weaker than those for **2Y** and **2Lu**. In the case of **2La**, this observation aligns with the UV-vis-NIR spectra (Fig. S37–S40) of the isolated materials, which show a lower radical content, whereas for **2Tm**, it does not. These spectra have poor resolution; that of **2Y** has partially resolved structure, which we have been unable to model assuming a single species,

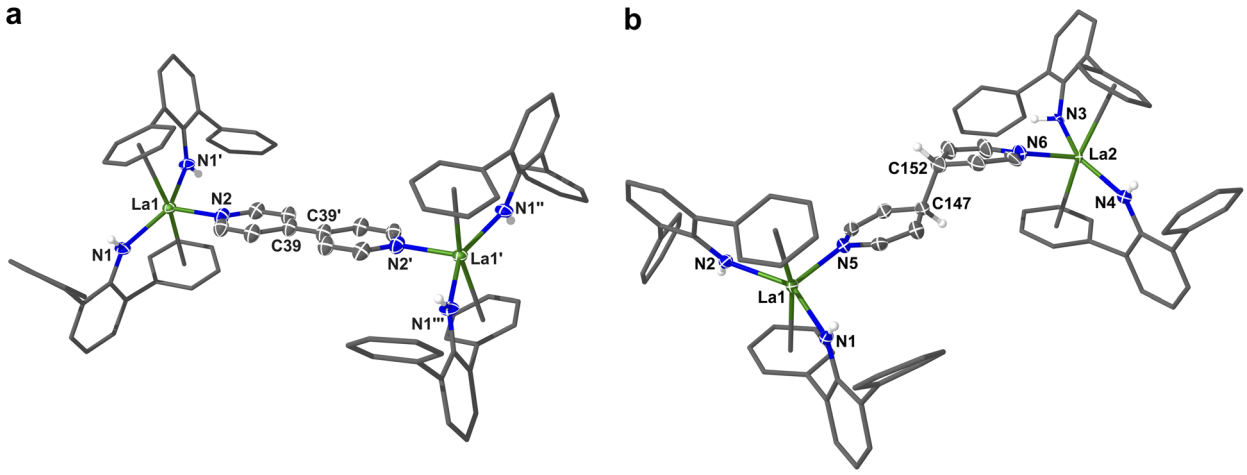

Fig. 4 Molecular structures of (a) [{La^{III}(NHAr^{iPr6})$_2$}$_2$(μ-N$_2$C$_{10}$H$_8$)] (**2La**) and (b) [{La^{III}(NHAr^{iPr6})$_2$}$_2$(μ-N$_2$C$_{10}$H$_{10}$)] (**3La**). Ellipsoids set at 30% probability. H-atoms except those on N–H groups are omitted for clarity, along with lattice solvents and ligand isopropyl groups.

hence it is likely due to small amounts of an oxidised form of **2M** together with dissociation products.

On one occasion during the preparation of **2Y** using an excess of 4,4′-bipyridine, several blue-purple crystals of a tetrameric complex, [{Y^{III}(NHAr^{iPr6})$_2$(μ-N$_2$C$_{10}$H$_{10}$)}$_4$] (**4**) were isolated – Fig. 5 shows the molecular structure (see Fig. S9 for full structural parameters). Complex **4** crystallised in the cubic space group $I\bar{4}3d$ ($Z' = 1/4$). Each Y-centre is 4-coordinate and adopts a pseudo-seesaw geometry coordinating to two terphenyl anilide ligands and two 4,4′-bipyridinyl radicals. The N$_{bipy}$–Y–N$_{bipy}$ angles of 88.67(15)° result in a twisted square arrangement of the four Y-atoms, which is significantly distorted from planarity (Fig. 5c). The Y–N$_{bipy}$ bond lengths (2.389(4) Å and 2.377(4) Å) are longer than in **2Y** (2.211(7) Å) by an amount larger than the difference in formal coordination number would suggest (*ca.* 0.05),[92] though both are significantly shorter than those with neutral 4,4′-bipyridine adducts.[84,86,93] The central C–C bond of the 4,4′-bipyridine moieties of 1.419(7) Å is longer than in **2Y** (1.355(18) Å), and the torsion angle between the two pyridyl units (7.8(2)°) is consistent with each 4,4′-bipyridine unit being singly reduced to its radical form. Therefore, complex **4** possesses four trivalent yttrium centres bridged by four 4,4′-bypridyl radicals.

The targeted synthesis of complex **4** on a larger scale was attempted through two routes: (i) the stoichiometric reaction between **1Y** and 4,4′-bipyridine; and (ii) the reaction between **2Y**

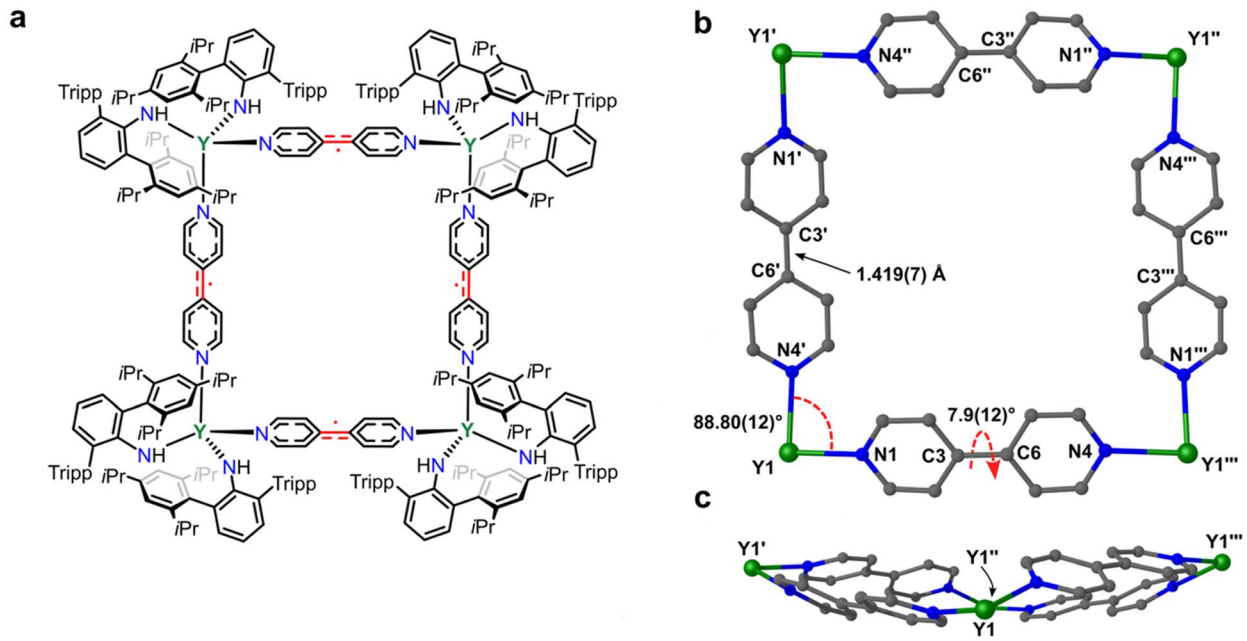

Fig. 5 (a) Schematic of complex **4** showing 4,4′-bipyridine radical bridges; (b) square-core of **4Y** showing only the Y atoms and 4,4′-bipyridine bridges with select distances and angles; (c) view of **4** along the Y1···Y1″ direction, showing the puckered conformation of the square-core in **4**.

and an additional equivalent of 4,4′-bipyridine. Both reactions produced intractable mixtures, and crystals suitable for SCXRD could not be grown from toluene, mesitylene, or Et_2O from −30 °C to room temperature.

Discussion

The measured M(III/II) reduction potentials of the **1M** (M = Y, La, Sm, Tm, Yb, Lu) complexes herein are all more anodic – the complexes are less reducing – than those of the $[RE^{II}(Cp')_3]^-$ series,[51] which reflects the differences in their electronic structure. No clear redox behaviour could be observed with **1Eu** save for an irreversible oxidation wave at anodic potentials. We suggest this is because the Eu(II) ion is significantly stabilised within the $\{M^{II}(NHAr^{iPr6})_2\}$ framework, and that ligand oxidation occurs at a more cathodic potential than metal oxidation. Some of us have previously reported the head-to-tail coupling of $\{NHAr^{iPr6}\}$ units during the attempted synthesis of $[Yb^{III}(NHAr^{iPr6})_2(I)]$ by salt elimination between $KNHAr^{iPr6}$ and $[Yb^{III}(I)_3(THF)_3]$, which instead resulted in the Yb(III) centre acting as an oxidant, giving HNC_6H_3-2,6-(2,4,6-iPr$_3$)-4-{HN=C_6H_3-2,6-(2,4,6-iPr$_3$)$_2$.[25] Given that the standard reduction potential for Yb(III/II) is more cathodic than that of Eu(III/II) – *i.e.* Eu(III) is more oxidising than Yb(III) – it follows that the electrochemical generation of Eu(III) could result in ligand oxidation here (Scheme 3a).

In **1Y**[24,25] and **1La**,[25] computational and spectroscopic data show the unpaired electron resides in a singly occupied molecular orbital (SOMO) resembling a δ-bond between the metal and flanking Tripp rings, whereas in divalent *tris*-Cp′ complexes, the SOMO resembles a non-bonding $\{(n+1)s(nd_z^2)\}$ hybrid atomic orbital. The bonding interaction stabilises the SOMO, which is reflected in the reduction potentials of **1Y**, **1La**, and **1Lu**. In the case of the Sm(III/II), Tm(III/II), and Yb(III/II) couples in **1M** and the tris-Cp′ complexes, both series follow the trend of their standard reduction potentials, but again, the **1M** complexes are less reducing. In this case, it reflects the fact that the **1M** complexes are neutral, whereas the $[RE^{II}(Cp')_3]^-$ complexes are electron-rich anions.[51]

Additional reduction events were found in cyclic voltammograms of the **1M** complexes (save **1Eu**), with potentials that trend opposite to the M(III/II) couples – *i.e.* the second event with **1Yb** is the most cathodic, and with **1Y** it is the most anodic. This order correlates with the f → d promotion energy for these ions (where applicable),[95,96] and we propose that it involves the reduction of one of the flanking Tripp groups, which subsequently forms a δ-bond to the metal centre *via* metal d-orbitals (Scheme 3b). In the case of **1Y**, **1La**, and **1Lu**, this could involve the formation of a closed-shell $\{Tripp\}^{2-}$ group, similar to the Ti(IV) complex $[Ti^{IV}(NHAr^{iPr6})_2]$.[94] With **1Sm**, **1Tm**, and **1Yb**, the vacant metal-based orbitals with appropriate symmetry are much higher in energy.

The data reveal an apparent incongruity between the measured reduction potentials and the observed chemical reducing power of the **1M** series. Complexes **1Y**, **1La**, and **1Lu** appear sufficiently reducing to access the $[naphthalene]^{0/-}$ ($E_{1/2}$ = −2.2 V *vs.* $[Fc]^{+/0}$) and $[anthracene]^{0/-}$ ($E_{1/2}$ = −1.9 V *vs.* $[Fc]^{+/0}$) couples,[68] but no reaction was observed with either (Fig. S142–S147); and none of the **1M** complexes show M(III/II) couples sufficiently negative for the reduction of pyridine or the double-reduction of 4,4′-bipyridine – by cyclic voltammetry (Fig. 2 and Scheme 1) – yet several are competent in reductions of the latter two *N*-heterocycles. Some of us have previously shown that small changes in the M···Tripp distances in **1Y** led to large differences in the degree to which the SOMO is localised on the metal, with larger distances increasing the metal localisation.[25] Furthermore, these data also suggested that, at least in the case of **1Y**, the metal centre does not coordinate 2-MeTHF.[25] While our electrochemical measurements were performed in THF, these complexes may also be crystallised in the presence of THF without apparent coordination.[24] Therefore, we suggest that the measured reduction potentials for **1M** likely correspond to the structures in solution where the $\{M^{II}(Tripp)_2\}$ core is unperturbed and similar to the structures from SCXRD.

Ab initio calculations on **1Y** using three different geometries: (i) coordinates derived from the SCXRD structures with H-atom positions optimised (**1Y-SCXRD**);[25] (ii) using coordinates optimised starting with the geometry of **1La**, such that a single Y··· Tripp interaction remains (**1Y-Opt**);[25] (iii) using the coordinates

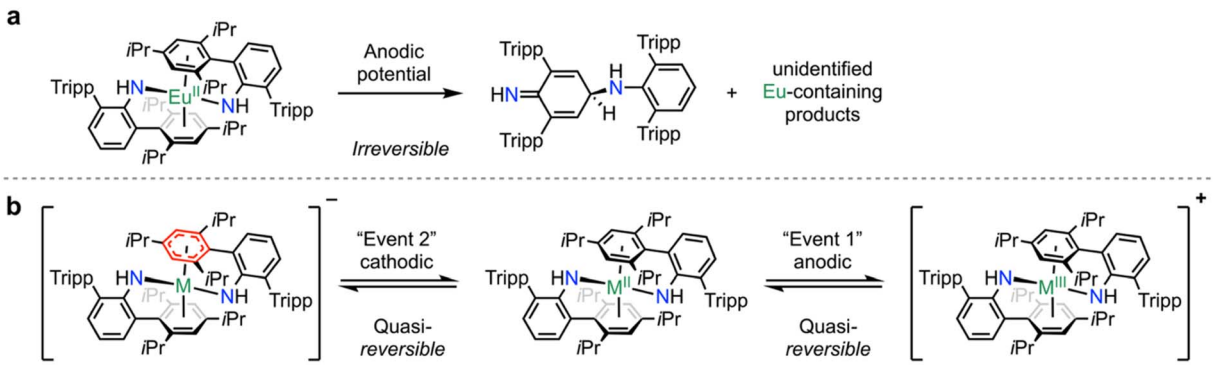

Scheme 3 Illustrations of the observed electrochemical processes seen with: (a) **1Eu**; and (b) other **1M** complexes (M = Y, La, Sm, Tm, Yb). The red {Tripp} ring indicates that the partitioning of charge between the metal centre and the arene ring is not known. Limiting ionic bonding descriptors: M(III) with $\{Tripp\}^{2-}$ or M(II) with $\{Tripp\}^{\bullet-}$ are possible, with the former resembling the case of $[Ti^{IV}(NHAr^{iPr6})_2]$.[94]

for one half of **2Y** with the {4,4′-bipyridine}$^{2-}$ removed (**1Y@2Y**; see SI Section 11 and Table S16). These revealed significant increases in the natural spin density at the metal,[97] and in the metal character of the SOMO as the {Y^{II}(Tripp)$_2$} core is progressively disrupted. This is shown schematically in Scheme 4, and accounts for the coordination-induced reduction seen in the **2M** and **3M** series.

Here, we suggest that the change in the {M^{II}(Tripp)$_2$} shown above not only alters the distribution of spin in the complexes, but also the M(III/II) reduction potential relative to the case in which the {M^{II}(Tripp)$_2$} core remains intact. Some **1M** complexes have already been shown to reduce P_4 to $(P_4)^{2-}$ (reduction potential reported between −1.53 and −1.98 V),[98,99] and cleave *t*BuNC to give $(CN)^-$.[24] In both cases, the reduced small molecules have heteroatom lone pairs that may coordinate to the metal centre, thereby disrupting the {M^{II}(Tripp)$_2$} core in the **1M** complexes. In the presence of reducible Lewis-basic molecules such as 4,4′-bipyridine and pyridine, the {M^{II}(Tripp)$_2$} core is disrupted, which increases the degree of metal-localisation in the SOMO to the point where electron transfer occurs.

The reduction of pyridine by **1Y**, **1La**, **1Tm**, and **1Lu** to give [{M^{III}(NHAr^{iPr6})$_2$}$_2$(μ-$N_2C_{10}H_{10}$)] (**3M**, M = Y, La, Tm, Lu) is similar to that of other formally low oxidation state complexes with electropositive metals,[46–48] or low oxidation state synthons.[35,100,101] Solutions of **3M** remain unchanged over the course of days or weeks by ^{1}H NMR spectroscopy, which contrasts the thorium complex [{Th^{IV}(Cp′)$_3$}$_2$(μ-$N_2C_{10}H_{10}$)] (Cp′ = {C_5H_3-1,3-(SiMe$_3$)$_2$}), which slowly reverts to the Th(III) precursor and unknown byproducts over time.[49] Similarly, the double-reduction of 4,4′-bipyridine to give bimetallic species bridged by the 4,4′-bipyridine dianion, as with [{M^{III}(NHAr^{iPr6})$_2$}$_2$(μ-$N_2C_{10}H_{10}$)] (**2M**, M = Y, La, Tm, Lu), is well-precedented.[49,67,82,101,102]

During the course of isolating **2Y**, **2Tm**, and **2Lu**, it became apparent that while SCXRD and NMR spectroscopic data suggested the bridging 4,4′-bipyridine moiety was doubly reduced due to the short C–C bond length and diamagnetic NMR spectra (except for **2Tm**), UV-vis-NIR and EPR spectroscopies of isolated crystalline material suggested the presence of a radical impurity. UV-vis-NIR and NMR titration studies subsequently showed that the **2M** complexes (M = Y, Tm, Lu) react with additional equivalents of neutral 4,4′-bipyridine, as evidenced by the isolation of complex **4**, which results in trace quantities of radical species in isolated samples of **2M**. Crucially, the reaction pathway that gives **4** exists at substoichiometric concentrations of 4,4′-bipyridine. Complex **2La** appears unreactive to additional 4,4′-bipyridine. In **2La**, as in **1La** and **3La**, the metal centre retains close contact with two flanking Tripp rings from the ligands, whereas in **2Y**, **2Tm**, and **2Lu**, one of these coordinating Tripp groups moves away to accommodate the additional N donor. Despite the La(III) ion being the largest of the four,[92] it is somewhat softer and provides a better size match for the {M^{III}(Tripp)$_2$} cavity. This shields the La-centre from the approach of additional 4,4′-bipyridine ligands, and precludes the formation of higher-order aggregates. EPR spectroscopy of isolated **2M** samples did not show signals due to the precursor **1M** complexes over time, suggesting that **2M** and **1M** are not in equilibrium with each other.

Taken alongside the titration studies and the unreactivity of **2La** towards 4,4′-bipyridine, these data suggest that the formation of **4** proceeds stepwise, requiring the initial formation of **2M**, followed by coordination and electron transfer to additional equivalents of 4,4′-bipyridine. Tetrameric radical-bridged lanthanide complexes using the 1,4-pyrazine[103] ($C_4H_4N_2$, M = Gd, Dy, Yb) and 1,2,4,5-tetrazene[104] ($C_2H_2N_4$, M = Tb) radicals have been reported, which all exhibit a similar square-like arrangement of the four lanthanide metals. Intriguingly, the Gd(III) and Dy(III) pyrazine complexes can be isolated in both the dimeric form, like **2M**, or as tetrameric species, like **4**, either by careful control of the stoichiometry or by dissolution in polar solvents.

Attempts to isolate crystalline samples of complex **4** on a larger scale were unsuccessful. However, this agrees with the solution behaviour described above. The UV-vis-NIR titration experiments show that mixtures of **1M** (M = Y, La, Tm, Lu) and 4,4′-bipyridine rapidly form new species even when extremely low equivalents of 4,4′-bipyridine are added – the spectra show broad and strong absorbances across the UV-vis range. As

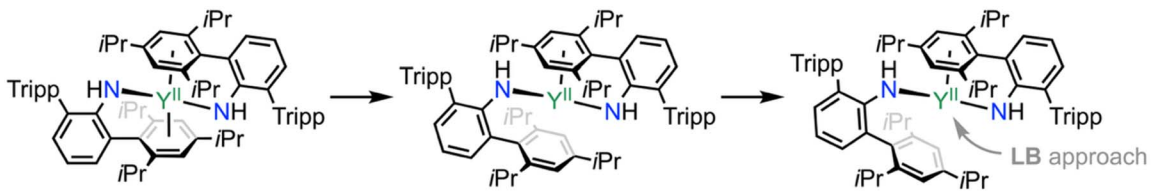

	1Y-SCXRD	1Y-Opt	1Y@2Y
Y···Tripp	2.448 Å 2.448 Å	2.894 Å 2.247 Å	3.317 Å 2.602 Å
Y nat. spin dens.	0.125	0.195	0.792
Y MO contribn.	18.3%	25.5%	74.3%

Scheme 4 Displacement of the {M^{II}(Tripp)$_2$} core by a strong Lewis base increases metal spin density and contribution to the SOMO, and ultimately results in coordination-induced reduction of the Lewis base. **1Y-SCXRD** refers to coordinates from the SXRD study of **1Y** with the H-atom positions optimised. **1Y-Opt** refers to the geometry obtained after optimising **1Y** using the coordinates for **1La** as a starting point, and it resides at a local minimum by vibrational analysis.[25] **1Y@2Y** refers to the coordinates from the {Y(Tripp)$_2$} unit in **2Y**, with the rest of the molecule removed, and the H-atom positions optimised.

greater equivalents of 4,4′-bipyridine are added to **1Y**, **1Tm** or **1Lu**, new species form, which show somewhat sharper features in the UV-vis range. In the case of **1La**, the UV-vis-NIR titration data show that the addition of 4,4′-bipyridine beyond that required to form **2La** does not substantially alter the UV-vis spectrum; this data, therefore, provides a spectroscopic handle for the $\{4,4'\text{-bipyridine}\}^{2-}$ dianion in our system (Fig. S150). Revisiting the UV-vis-NIR titration data for **1Y**, **1Tm**, and **1Lu** shows that the broad spectral features we attribute to $\{4,4'\text{-bipyridine}\}^{2-}$ are apparent with low equivalents of 4,4′-bipyridine. However, at 0.23 (**1Y**), 0.11 (**1Tm**), or 0.13 (**1Lu**) equivalents of 4,4′-bipyridine, respectively, the UV-vis-NIR data already show the same sharper spectral features that simply continue to grow in strength with additional 4,4′-bipyridine (Fig. S149, S151, and S152). These sharper features are associated with the $\{4,4'\text{-bipyridyl}\}^{\bullet-}$ radical anion,[62–66] which is also present in **4**.

In sum, we suggest that when 4,4′-bipyridine is added to solutions of **1M** (M = Y, La, Tm, Lu), the components react rapidly to form **2M**, even at substoichiometric quantities of 4,4′-bipyridine. In the case of **1La**, the product complex (**2La**) appears almost unreactive to 4,4′-bipyridine except at high ratios (approaching 1 : 1), and so as further 4,4′-bipyridine is added, the formation of additional **2La** is all that is observed as the remaining **1La** is consumed. With **1Y**, **1Tm**, and **1Lu**, the product complexes (**2Y**, **2Tm**, and **2Lu**) appear to react with 4,4′-bipyridine at a similar rate to the **1M** complexes, giving rise to a mixture of species, such as **4**, and possibly others that are less crystalline and which we have been unable to characterise.

Conclusions

Cyclic voltammetry of the divalent terphenyl anilide rare earth complexes $[M^{II}(NHAr^{iPr6})_2]$ (**1M**, M = Y, La, Sm, Tm, Yb, Lu) using an internal electrochemical standard shows their M(III/II) reduction couples span the range −2.32 V to −1.20 V (*vs.* $[Fe(Cp)_2]^{+/0}$) are more anodic than related divalent rare earth complexes. The Eu(II) complex showed no electrochemical response, regardless of whether the experiments were performed in the light or dark. Electrochemical measurements do not necessarily correlate with chemical reducing power; therefore, the reactivity of all complexes towards pyridine, 4,4′-bipyridine, naphthalene, and anthracene was explored, given their well-established reduction chemistry.

While the Sm(II), Eu(II), and Yb(II) complexes were unreactive towards 4,4′-bipyridine and pyridine, the Y(II), La(II), Tm(II), and Lu(II) complexes were found to reduce 4,4′-bipyridine to its dianion in bimetallic $[\{M^{III}(NHAr^{iPr6})_2\}_2(\mu\text{-}N_2C_{10}H_8)]$ (**1M**, M = Y, La, Tm, Lu), and promote the reduction and subsequent C–C coupling of pyridine to give bimetallic $[\{M^{III}(NHAr^{iPr6})_2\}_2(\mu\text{-}N_2C_{10}H_{10})]$ (**3M**, M = Y, La, Tm, Lu). The reduction potentials of 4,4′-bipyridine and pyridine are more cathodic than the measured M(III/II) couples of the precursor complexes. As none of the divalent precursor complexes showed reactivity towards naphthalene or anthracene, both of which are more easily reduced than pyridine, these serve as examples of coordination-induced reduction.

Single-crystal X-ray diffraction and NMR spectroscopy data indicated full reduction to the 4,4′-bipyridine dianion for all **2M** complexes; however, UV-vis-NIR and EPR spectroscopy indicated the trace quantities of the 4,4′-bipyridyl radical anion in isolated samples of **2Y**, **2Tm**, and **2Lu**. UV-vis-NIR and NMR titration studies showed that **2Y**, **2Tm**, and **2Lu** react with additional equivalents of 4,4′-bipyridine, even at substoichiometric ratios, and in one instance, several crystals of the tetrametallic complex $[\{Y^{III}(NHAr^{iPr6})_2\}_4(\mu\text{-}N_2C_{10}H_8)_4]$ (**4**) were isolated, which contains four bridging 4,4′-bipyridine radical anions. Complex **2La** was inert towards additional 4,4′-bipyridine until a large excess was added.

This study highlights the value of assessing rare-earth redox chemistry using both chemical and electrochemical methods and describes a case in which the results are starkly contrasting.

Author contributions

C. A. P. G. provided the original concept. R. E. M. and H. S. synthesised and characterised the complexes. R. E. M. collected, solved, and refined the single-crystal XRD data, and G. F. S. W. performed final refinement and validation. B. L. L. R performed electrochemical measurements and data analysis. I. J. C. performed EPR spectroscopy measurements, E. J. L. M. supervised the EPR measurements and data interpretation. C. A. P. G. performed DFT calculations and interpretation. R. E. M. wrote the first draft of the manuscript, and C. A. P. G. revised the manuscript with contributions from all other authors.

Conflicts of interest

There are no conflicts to declare.

Data availability

CCDC 2478500 (**2Y**), 2478501 (**2La**), 2478502 (**2Tm**), 2478503 (**2Lu**), 2478504 (**3Y**), 2478505 (**3La**), 2478506 (**3Tm**), 2478507 (**3Lu**), and 2478508 (**4**) contain the supplementary crystallographic data for this paper.[106a–i]

Raw instrument and calculation outputs are deposited at FigShare (DOI: 10.48420/31748533). All other data are available in the supplementary information (SI). A preprint of this article was previously deposited on ChemRxiv.[105] Supplementary information is available. See DOI: https://doi.org/10.1039/d6sc03059a.

Acknowledgements

We thank the Royal Society for a University Research Fellowship (URF\211271 to C. A. P. G.). The EPSRC (EP/Y006534/1) is also thanked for postdoctoral funding (B. L. L. R). We acknowledge the University of Manchester School of Natural Sciences and the EPSRC DTP (EP/W524347/1 to R. E. M. and I. J. C.) for funding. We thank the EPSRC UK EPR National Research Facility (EP/W014521/1, EP/V035231/1, EPS033181/1). We acknowledge funding from the EPSRC (EP/K039547/1, EP/V007580/1, and EP/P001386/1 for NMR spectroscopy and X-ray diffraction). C. A. P.

G. thanks the Computational Shared Facility at the University of Manchester for support. Elemental analyses were performed at the UoM by Mr Martin Jennings and Ms Anne Davies. Mr David Marshall and Mr Steven Green produced bespoke glassware at the University of Manchester.

References

1 F. Nief, *Dalton Trans.*, 2010, **39**, 6589–6598.
2 M. N. Bochkarev, I. L. Fedushkin, A. A. Fagin, T. V. Petrovskaya, J. W. Ziller, R. N. R. Broomhall-Dillard and W. J. Evans, *Angew. Chem., Int. Ed.*, 1997, **36**, 133–135.
3 W. J. Evans, N. T. Allen and J. W. Ziller, *J. Am. Chem. Soc.*, 2000, **122**, 11749–11750.
4 M. N. Bochkarev, I. L. Fedushkin, S. Dechert, A. A. Fagin and H. Schumann, *Angew. Chem., Int. Ed.*, 2001, **40**, 3176–3178.
5 W. J. Evans, *Organometallics*, 2016, **35**, 3088–3100.
6 H. Kwon, K. R. McClain, J. K. Staab, P. W. Smith, B. G. Harvey, M. P. Erodici, S. J. Teat, T. D. Harris, S. Minasian, N. F. Chilton and J. R. Long, *J. Am. Chem. Soc.*, 2026, **148**, 6354–6364.
7 D. N. Huh, S. R. Ciccone, S. Bekoe, S. Roy, J. W. Ziller, F. Furche and W. J. Evans, *Angew. Chem., Int. Ed.*, 2020, **59**, 16141–16146.
8 M. E. Fieser, M. R. MacDonald, B. T. Krull, J. E. Bates, J. W. Ziller, F. Furche and W. J. Evans, *J. Am. Chem. Soc.*, 2015, **137**, 369–382.
9 H. P. Beck and Z. Naturforsch, *J. Chem. Sci.*, 1976, **31**, 1548–1549.
10 H. P. Beck and M. Schuster, *J. Solid State Chem.*, 1992, **100**, 301–306.
11 D. H. Woen and W. J. Evans, in *Handbook on the Physics and Chemistry of Rare Earths*, eds. J.-C. G. Bünzli and V. K. Pecharsky, Elsevier, 2016, vol. 50, pp. 337–394.
12 A. Rajabi, D. K. Nguyen, R. Grotjahn and F. Furche, *Inorg. Chem.*, 2025, **64**, 9477–9490.
13 P. B. Hitchcock, M. F. Lappert, L. Maron and A. V. Protchenko, *Angew. Chem., Int. Ed.*, 2008, **47**, 1488–1491.
14 M. R. MacDonald, J. W. Ziller and W. J. Evans, *J. Am. Chem. Soc.*, 2011, **133**, 15914–15917.
15 M. R. MacDonald, J. E. Bates, M. E. Fieser, J. W. Ziller, F. Furche and W. J. Evans, *J. Am. Chem. Soc.*, 2012, **134**, 8420–8423.
16 M. R. MacDonald, J. E. Bates, J. W. Ziller, F. Furche and W. J. Evans, *J. Am. Chem. Soc.*, 2013, **135**, 9857–9868.
17 C. A. Gould, K. R. McClain, J. M. Yu, T. J. Groshens, F. Furche, B. G. Harvey and J. R. Long, *J. Am. Chem. Soc.*, 2019, **141**, 12967–12973.
18 K. R. McClain, C. A. Gould, D. A. Marchiori, H. Kwon, T. T. Nguyen, K. E. Rosenkoetter, D. Kuzmina, F. Tuna, R. D. Britt, J. R. Long and B. G. Harvey, *J. Am. Chem. Soc.*, 2022, **144**, 22193–22201.
19 D. X. Ngo, K. R. McClain, J. Hrubý, Y. J. Franzke, K. Kundu, H. Kwon, C. A. Gould, B. G. Harvey, S. Hill and J. R. Long, *J. Am. Chem. Soc.*, 2025, **147**, 13799–13807.
20 D. H. Woen, G. P. Chen, J. W. Ziller, T. J. Boyle, F. Furche and W. J. Evans, *Angew. Chem., Int. Ed.*, 2017, **56**, 2050–2053.
21 K. Gilbert-Bass, C. R. Stennett, R. Grotjahn, J. W. Ziller, F. Furche and W. J. Evans, *Chem. Commun.*, 2024, **60**, 4601–4604.
22 Y. Wang, J. Liang, C. Deng, R. Sun, P.-X. Fu, B.-W. Wang, S. Gao and W. Huang, *J. Am. Chem. Soc.*, 2023, **145**, 22466–22474.
23 M. E. Fieser, C. T. Palumbo, H. S. La Pierre, D. P. Halter, V. K. Voora, J. W. Ziller, F. Furche, K. Meyer and W. J. Evans, *Chem. Sci.*, 2017, **8**, 7424–7433.
24 R. Jena, F. Benner, F. Delano, D. Holmes, J. McCracken, S. Demir and A. L. Odom, *Chem. Sci.*, 2023, **14**, 4257–4264.
25 R. E. MacKenzie, T. Hajdu, J. A. Seed, G. F. S. Whitehead, R. W. Adams, N. F. Chilton, D. Collison, E. J. L. McInnes and C. A. P. Goodwin, *Chem. Sci.*, 2024, **15**, 15160–15169.
26 P.-B. Jin, Q.-C. Luo, G. K. Gransbury, I. J. Vitorica-Yrezabal, T. Hajdu, I. Strashnov, E. J. L. McInnes, R. E. P. Winpenny, N. F. Chilton, D. P. Mills and Y.-Z. Zheng, *J. Am. Chem. Soc.*, 2023, **145**, 27993–28009.
27 D. Frick, E. Pross, R. Köppe and P. W. Roesky, *Angew. Chem., Int. Ed.*, 2025, **64**, e202503403.
28 M. Zhu, T. Li, Z. Chai, J. Wei, Z.-J. Lv and W.-X. Zhang, *Inorg. Chem. Front.*, 2023, **10**, 630–637.
29 P. Ghana, T. P. Spaniol and J. Okuda, *Chem.–Asian J.*, 2021, **16**, 3170–3178.
30 C. Yu, J. Liang, C. Deng, G. Lefèvre, T. Cantat, P. L. Diaconescu and W. Huang, *J. Am. Chem. Soc.*, 2020, **142**, 21292–21297.
31 C. T. Palumbo, L. E. Darago, M. T. Dumas, J. W. Ziller, J. R. Long and W. J. Evans, *Organometallics*, 2018, **37**, 3322–3331.
32 S. K. Thakur, J. Langer and S. Harder, *Chem.–Eur. J.*, 2025, **31**, e02710.
33 S. K. Thakur, N. Roig, R. Monreal-Corona, J. Langer, M. Alonso and S. Harder, *Angew. Chem., Int. Ed.*, 2024, **63**, e202405229.
34 P. Deng, Y. Gao, X. Kang and J. Cheng, *Inorg. Chem.*, 2025, **64**, 14313–14323.
35 W. Huang, S. I. Khan and P. L. Diaconescu, *J. Am. Chem. Soc.*, 2011, **133**, 10410–10413.
36 W. Huang and P. L. Diaconescu, *Dalton Trans.*, 2015, **44**, 15360–15371.
37 W. Huang and P. L. Diaconescu, *Chem. Commun.*, 2012, **48**, 2216–2218.
38 P.-B. Jin, Q.-C. Luo, G. K. Gransbury, R. E. P. Winpenny, D. P. Mills and Y.-Z. Zheng, *Chem. Sci.*, 2025, **16**, 1907–1924.
39 W. J. Evans, T. A. Ulibarri and J. W. Ziller, *J. Am. Chem. Soc.*, 1988, **110**, 6877–6879.
40 A. J. Ryan, S. g. Balasubramani, J. W. Ziller, F. Furche and W. J. Evans, *J. Am. Chem. Soc.*, 2020, **142**, 9302–9313.
41 W. J. Evans, J. W. Grate, L. A. Hughes, H. Zhang and J. L. Atwood, *J. Am. Chem. Soc.*, 1985, **107**, 3728–3730.
42 T. Simler, K. N. McCabe, L. Maron and G. Nocton, *Chem. Sci.*, 2022, **13**, 7449–7461.
43 Z. Du, W. Li, X. Zhu, F. Xu and Q. Shen, *J. Org. Chem.*, 2008, **73**, 8966–8972.

44 C. J. Weiss, S. D. Wobser and T. J. Marks, *Organometallics*, 2010, **29**, 6308–6320.
45 W. J. Evans and D. K. Drummond, *J. Am. Chem. Soc.*, 1989, **111**, 3329–3335.
46 S. Labouille, F. Nief, X. F. Le Goff, L. Maron, D. R. Kindra, H. L. Houghton, J. W. Ziller and W. J. Evans, *Organometallics*, 2012, **31**, 5196–5203.
47 A. B. Chung, A. J. Ryan, M. Fang, J. W. Ziller and W. J. Evans, *Inorg. Chem.*, 2021, **60**, 15635–15645.
48 F. Jaroschik, F. Nief, X. F. Le Goff and L. Ricard, *Organometallics*, 2007, **26**, 3552–3558.
49 A. Formanuik, F. Ortu, J. Liu, L. E. Nodaraki, F. Tuna, A. Kerridge and D. P. Mills, *Chem.–Eur. J.*, 2017, **23**, 2290–2293.
50 M. E. Fieser, M. G. Ferrier, J. Su, E. Batista, S. K. Cary, J. W. Engle, W. J. Evans, J. S. Lezama Pacheco, S. A. Kozimor, A. C. Olson, A. J. Ryan, B. W. Stein, G. L. Wagner, D. H. Woen, T. Vitova and P. Yang, *Chem. Sci.*, 2017, **8**, 6076–6091.
51 M. T. Trinh, J. C. Wedal and W. J. Evans, *Dalton Trans.*, 2021, **50**, 14384–14389.
52 R. R. Gagne, C. A. Koval and G. C. Lisensky, *Inorg. Chem.*, 1980, **19**, 2854–2855.
53 I. Noviandri, K. N. Brown, D. S. Fleming, P. T. Gulyas, P. A. Lay, A. F. Masters and L. Phillips, *J. Phys. Chem. B*, 1999, **103**, 6713–6722.
54 J. E. Niklas, M. I. Duffy and H. S. La Pierre, *Inorg. Chem.*, 2026, **65**, 3758–3770.
55 J. R. Aranzaes, M.-C. Daniel and D. Astruc, *Can. J. Chem.*, 2006, **84**, 288–299.
56 L. R. Morss, *Chem. Rev.*, 1976, **76**, 827–841.
57 M. Jordan, W. Saak, D. Haase and R. Beckhaus, *Organometallics*, 2010, **29**, 5859–5870.
58 K. B. Wiberg and T. P. Lewis, *J. Am. Chem. Soc.*, 1970, **92**, 7154–7160.
59 B. J. Tabner and J. R. Yandle, *J. Chem. Soc. A*, 1968, 381–388.
60 S. Perera, X. Li, M. Soler, A. Schultz, C. Wesdemiotis, C. N. Moorefield and G. R. Newkome, *Angew. Chem., Int. Ed.*, 2010, **49**, 6539–6544.
61 H.-J. Li, R. Feng, X. Shi, J. Wei and Z. Xi, *Dalton Trans.*, 2022, **51**, 15696–15702.
62 V. Kalyanaraman, C. N. R. Rao and M. V. George, *J. Chem. Soc. B*, 1971, 2406–2409.
63 G. Buntinx, P. Valat, V. Wintgens and O. Poizat, *J. Phys. Chem.*, 1991, **95**, 9347–9352.
64 O. Poizat, G. Buntinx, P. Valat, V. Wintgens and M. Bridoux, *J. Phys. Chem.*, 1993, **97**, 5905–5910.
65 H. Kihara and Y. Gondo, *J. Raman Spectrosc.*, 1986, **17**, 263–267.
66 C. B. Benda, T. F. Fässler and Z. Naturforsch, *J. Chem. Sci.*, 2014, **69**, 1119–1123.
67 H. A. Spinney, C. R. Clough and C. C. Cummins, *Dalton Trans.*, 2015, **44**, 6784–6796.
68 S. Bank and D. A. Juckett, *J. Am. Chem. Soc.*, 1976, **98**, 7742–7746.
69 I. L. Fedushkin, M. N. Bochkarev, S. Dechert and H. Schumann, *Chem.–Eur. J.*, 2001, **7**, 3558–3563.
70 M. N. Bochkarev, *Chem. Rev.*, 2002, **102**, 2089–2118.
71 C. M. Kotyk, M. E. Fieser, C. T. Palumbo, J. W. Ziller, L. E. Darago, J. R. Long, F. Furche and W. J. Evans, *Chem. Sci.*, 2015, **6**, 7267–7273.
72 C. M. Kotyk, M. R. MacDonald, J. W. Ziller and W. J. Evans, *Organometallics*, 2015, **34**, 2287–2295.
73 C. T. Palumbo, M. E. Fieser, J. W. Ziller and W. J. Evans, *Organometallics*, 2017, **36**, 3721–3728.
74 P. B. Hitchcock, M. F. Lappert and A. V. Protchenko, *J. Am. Chem. Soc.*, 2001, **123**, 189–190.
75 F. G. N. Cloke and N. Tsoureas, in *Comprehensive Organometallic Chemistry IV*, eds. G. Parkin, K. Meyer and D. O'hare, Elsevier, Oxford, 2022, pp. 405–459.
76 R. P. Kelly, D. Toniolo, F. F. Tirani, L. Maron and M. Mazzanti, *Chem. Commun.*, 2018, **54**, 10268–10271.
77 W. J. Evans, S. L. Gonzales and J. W. Ziller, *J. Am. Chem. Soc.*, 1994, **116**, 2600–2608.
78 I. L. Fedushkin, V. I. Nevodchikov, M. N. Bochkarev, S. Dechert and H. Schumann, *Russ. Chem. Bull.*, 2003, **52**, 154–159.
79 M. N. Bochkarev, I. L. Fedushkin, A. A. Fagin, H. Schumann and J. Demtschuk, *Chem. Commun.*, 1997, 1783–1784.
80 W. T. Carnall and P. R. Fields, in *Lanthanide/Actinide Chemistry*, American Chemical Society, 1967, vol. 71, ch. 7, pp. 86–101.
81 M. Irwin, T. Krämer, J. E. McGrady and J. M. Goicoechea, *Inorg. Chem.*, 2011, **50**, 5006–5014.
82 M. S. Denning, M. Irwin and J. M. Goicoechea, *Inorg. Chem.*, 2008, **47**, 6118–6120.
83 B. N. Long, M. J. Beltran-Leiva, J. M. Sperling, T. N. Poe, C. Celis-Barros and T. E. Albrecht-Schonzart, *Nat. Commun.*, 2023, **14**, 3774.
84 P. R. Matthes, J. Nitsch, A. Kuzmanoski, C. Feldmann, A. Steffen, T. B. Marder and K. Müller-Buschbaum, *Chem.–Eur. J.*, 2013, **19**, 17369–17378.
85 J. C. Muñoz, A. M. Atria, R. Baggio, M. T. Garland, O. Peña and C. Orrego, *Inorg. Chim. Acta*, 2005, **358**, 4027–4033.
86 D. Barisic, D. Schneider, C. Maichle-Mössmer and R. Anwander, *Angew. Chem., Int. Ed.*, 2019, **58**, 1515–1518.
87 A. Czylkowska, D. Czakis-Sulikowska, R. Kruszyński and M. Markiewicz, *Struct. Chem.*, 2010, **21**, 415–423.
88 S. Khanjani and A. Morsali, *J. Coord. Chem.*, 2009, **62**, 3343–3350.
89 K. C. Jantunen, B. L. Scott, J. C. Gordon and J. L. Kiplinger, *Organometallics*, 2007, **26**, 2777–2781.
90 G. R. Giesbrecht, G. E. Collis, J. C. Gordon, D. L. Clark, B. L. Scott and N. J. Hardman, *J. Organomet. Chem.*, 2004, **689**, 2177–2185.
91 S. Arndt, B. R. Elvidge, P. M. Zeimentz, T. P. Spaniol and J. Okuda, *Organometallics*, 2006, **25**, 793–795.
92 R. D. Shannon, *Acta Crystallogr., Sect. A*, 1976, **32**, 751–767.
93 J. R. Thomas, E. A. Murray-Nobbs, R. A. Mole, M. J. Giansiracusa and S. A. Sulway, *Inorg. Chem.*, 2025, **64**, 21489–21500.
94 J. N. Boynton, J. D. Guo, F. Grandjean, J. C. Fettinger, S. Nagase, G. J. Long and P. P. Power, *Inorg. Chem.*, 2013, **52**, 14216–14223.

95 P. Dorenbos, *J. Lumin.*, 2000, **91**, 91–106.
96 P. Dorenbos, *J. Phys.: Condens. Matter*, 2003, **15**, 575–594.
97 E. D. Glendening, C. R. Landis and F. Weinhold, *J. Comput. Chem.*, 2019, **40**, 2234–2241.
98 R. Jena, F. Benner, R. J. Staples, S. Demir and A. L. Odom, *Inorg. Chem.*, 2025, **64**, 20643–20651.
99 I. M. Osadchenko and A. P. Tomilov, *Russ. J. Appl. Chem.*, 2006, **79**, 2033–2034.
100 D. K. Modder, C. T. Palumbo, I. Douair, F. Fadaei-Tirani, L. Maron and M. Mazzanti, *Angew. Chem., Int. Ed.*, 2021, **60**, 3737–3744.
101 J. R. Aguilar-Calderón, J. Murillo, A. Gomez-Torres, C. Saucedo, A. Jordan, A. J. Metta-Magaña, M. Pink and S. Fortier, *Organometallics*, 2020, **39**, 295–311.
102 D. K. Modder, R. Scopelliti and M. Mazzanti, *Inorg. Chem.*, 2024, 9527–9538.
103 N. Bajaj, N. Mavragani, A. A. Kitos, D. Chartrand, T. Maris, A. Mansikkamäki and M. Murugesu, *Chem*, 2024, **10**, 2484–2499.
104 N. Mavragani, A. A. Kitos, A. Mansikkamäki and M. Murugesu, *Chem. Sci.*, 2024, **15**, 16234–16242.
105 R. E. MacKenzie, B. L. L. Réant, I. J. Cameron, H. M. Silver, G. F. S. Whitehead, E. J. L. McInnes and C. A. P. Goodwin, *ChemRxiv*, 2026, DOI: 10.26434/chemrxiv.15002040/v15002041.
106 (*a*) CCDC 2478500: Experimental Crystal Structure Determination, 2026, DOI: 10.5517/ccdc.csd.cc2p62mm; (*b*) CCDC 2478501: Experimental Crystal Structure Determination, 2026, DOI: 10.5517/ccdc.csd.cc2p62nn; (*c*) CCDC 2478502: Experimental Crystal Structure Determination, 2026, DOI: 10.5517/ccdc.csd.cc2p62pp; (*d*) CCDC 2478503: Experimental Crystal Structure Determination, 2026, DOI: 10.5517/ccdc.csd.cc2p62qq; (*e*) CCDC 2478504: Experimental Crystal Structure Determination, 2026, DOI: 10.5517/ccdc.csd.cc2p62rr; (*f*) CCDC 2478505: Experimental Crystal Structure Determination, 2026, DOI: 10.5517/ccdc.csd.cc2p62ss; (*g*) CCDC 2478506: Experimental Crystal Structure Determination, 2026, DOI: 10.5517/ccdc.csd.cc2p62tt; (*h*) CCDC 2478507: Experimental Crystal Structure Determination, 2026, DOI: 10.5517/ccdc.csd.cc2p62vv; (*i*) CCDC 2478508: Experimental Crystal Structure Determination, 2026, DOI: 10.5517/ccdc.csd.cc2p62ww.